# The Combretastatin Derivative (Cderiv), a Vascular Disrupting Agent, Enables Polymeric Nanomicelles to Accumulate in Microtumors

KATSUYOSHI HORI,[1] MASAMICHI NISHIHARA,[2] KOUICHI SHIRAISHI,[2] MASAYUKI YOKOYAMA[2,3]

[1]Division of Cancer Control, Department of Vascular Biology, Institute of Development, Aging and Cancer, Tohoku University, 4-1 Seiryomachi, Aoba-ku, Sendai, 980-0785 Miyagi, Japan

[2]Kanagawa Academy of Science and Technology, 3-2-1 Sakado, Takatsu-ku, Kawasaki, 213-0012 Kanagawa, Japan

[3]Medical Engineering Laboratory, Research Center for Medical Science, Jikei University School of Medicine, 3-25-8 Nishi-shinbashi, Minato-ku, 105-8461 Tokyo, Japan

*Received 4 June 2009; revised 29 October 2009; accepted 3 November 2009*

*Published online in Wiley InterScience (www.interscience.wiley.com). DOI 10.1002/jps.22038*

**ABSTRACT:** A previous study found almost no leakage of polymeric nanomicelles from vessels in microtumors. If such vessels become leaky, sufficient nanomedicines may be delivered to microtumors and large tumors. To create leaky vessels, a combretastatin derivative (Cderiv), a vascular disrupting agent, was used. Via vital microscopy with fluorescein isothiocyanate (FITC)-labeled nanomicelles, the effect of Cderiv pretreatment on changes in micelle extravasation was investigated. Whether such treatment would prolong microtumor retention of micelles was also examined. FITC-albumin was used for comparison. The degree of extravasation from intact vessels in microtumors (rat sarcoma LY80) was extremely low and comparable to that from normal vessels. Cderiv pretreatment (1 or 3 days before administration of FITC-labeled compounds) markedly enhanced extravasation of such nanomicelles and albumin from vessels that survived treatment and had restored blood flow. A high concentration of extravasated macromolecules remained even 24 h later in tissue areas whose microcirculatory function had collapsed. Tumors receiving 10 Gy irradiation 3 days before the macromolecules evidenced gradual removal of extravasated macromolecules, which did not accumulate in those areas, despite extravasation from tumor vessels. Our results strongly suggest that pretreatment with Cderiv is quite effective for maintaining microtumor concentrations of nanomicelles and albumin associated with anticancer or diagnostic drugs. © 2009 Wiley-Liss, Inc. and the American Pharmacists Association J Pharm Sci

**Keywords:** cancer; drug targeting; macromolecular drug delivery; micelle; polymeric drug carrier; albumin; combretastatin; irradiation; EPR effect; vital microscopy

## INTRODUCTION

In recent years, nanoparticles incorporating anticancer drugs have been developed as a technique for achieving selective drug delivery to solid tumors.[1–9] This therapeutic strategy is based on the hypothesis that particles larger than a specific size selectively extravasate from tumor vessels, because tumor vessels have wider intercellular gaps than normal vessels.[1,4,7]

Recently, however, by means of vital microscopic analysis with fluorescein isothiocyanate (FITC)-labeled polymeric micelles, the following results concerning extravasation and retention of micelles in tumors were obtained:[10] (i) polymeric micelles readily leaked from vessels at the interface between normal and tumor tissues and at the interface between tumor tissues and necrotic areas, with the latter interface showing markedly enhanced extravasation; (ii) polymeric micelles accumulated at a high concentration in necrotic tumors with circulatory dysfunction; and (iii) polymeric micelles barely extravasated from vessels in microtumors <2–3 mm in diameter that had no necrotic areas, and these micelles did not accumulate in such microtumors.

Findings (i) and (ii) are important phenomena for inducing the enhanced permeability and retention (EPR) effect[11–13] discovered by Maeda and Matsumura. Finding (iii), however, indicates that

*Correspondence to*: Katsuyoshi Hori (Telephone: 81-22-717-8532; Fax: 81-22-717-8533; E-mail: k-hori@idac.tohoku.ac.jp)

the EPR effect is not often seen in microtumors. This result suggests that microscopic metastatic foci may escape from the attack of nanomedicines that have encapsulated anticancer drugs. This extremely important problem influences survival of individuals who have cancer cells that survive in micrometastatic foci. Thus, to enhance the therapeutic ability of such drugs, the EPR effect must function not only in large tumors but also in microtumors.

To induce necrotic areas and leaky blood vessels in microtumors, a combretastatin derivative (Cderiv), (*Z*)-*N*-[2-methoxy-5-[2-(3,4,5-trimethoxyphenyl)vinyl] phenyl]-L-serinamide hydrochloride (formerly known as AC7700[14]) was used, because Cderiv selectively interrupts tumor blood flow, disrupts tumor vessels, and thereby causes necrosis of tumor tissue.[15–18] Such effects of Cderiv were observed in carcinogen-induced primary tumors[19] and transplanted tumors.[16,20] They were seen not only in subcutaneous tumors but also in tumors growing in internal organs, in lymph node metastases, and in microtumors <1 mm in diameter.[20] In addition, X-irradiation was used in the present study because it enhances the permeability of blood vessels while simultaneously damaging tumor tissues.[21] If the EPR effect of nanomedicines were enhanced by pretreatment with Cderiv or X-irradiation, advancements in cancer therapy and diagnosis may follow.

In the present study, we used FITC-labeled polymeric micelles and analyzed how extravasation and intratumor retention of such nanoparticles changed after pretreatment with Cderiv or X-irradiation. FITC-albumin was used as a comparison. The aim of the present study was to show that the EPR effect can effectively be induced in microtumors by causing the collapse of tumor microcirculatory function via pretreatment with Cderiv.

## MATERIALS AND METHODS

### Rats and Tumors

Male Donryu rats (Crj-Donryu; Nippon Charles-River, Yokohama, Japan), 7–8 weeks old and with an average weight of 220–250 g, were used for all experiments. Rats were bred and maintained in accordance with The Law (No. 105) and Notification (No. 6) issued by the Japanese Government. Specifically, they were comfortably housed in a ventilated, temperature-controlled (24 ± 1°C), specific pathogen-free environment on a bed of wood shavings, with food and water freely available and a 12-h light–dark cycle. Rats that were equipped with transparent chambers for vital microscopic observations (see below) were caged singly (cage volume, $30 \times 40 \times 25\ cm^3$).

A variant of Yoshida sarcoma, LY80, was used in the present experiments. This cell line, which can grow in ascites and in solid form, was maintained by successive i.p. transplantation. The transplantation rate of LY80 to Donryu rats was ~100%, without spontaneous regression.

All experimental protocols were reviewed by the Committee on the Ethics of Animal Experiments of Tohoku University and were carried out according to the Guidelines for Animal Experiments issued by Tohoku University.

### Anesthesia

Both pentobarbital sodium salt (Tokyo Kasei Kogyo Co., Tokyo, Japan) and enflurane (Abbott Laboratories, North Chicago, IL), given simultaneously, were used for anesthesia. Pentobarbital solution (50 mg/mL) was administered i.m., 10 min before the experiment, at a dose of 30 mg/kg, and supplemental doses (15 mg/kg i.m.) were given at 90-min intervals to maintain immobilization. Enflurane concentration was maintained at 1% in the inhaled gas, which was administered at a rate of 1 L/min by means of an anesthetic apparatus for small laboratory animals.[10]

### Implantation of Transparent Chambers and Tumor Transplantation

For *in vivo* analysis of extravasation of FITC-labeled compounds, transparent chambers were implanted, under aseptic conditions, in dorsal skin flaps of rats.[22] For tumor transplantation, a small fragment (~$0.1\ mm^3$) of solid tumor from a donor rat was transplanted onto the normal tissue in a transparent chamber while the chamber was being implanted in the dorsal skin flap. This transparent chamber enables observation of changes in the tumor vascular system, from angiogenesis to necrosis (for ~2 weeks).

### Microtumors

The term "microtumors" in the present study was defined as tumors <3 mm in diameter growing in the transparent chamber. Experiments on microtumors were usually performed 7–9 days after tumor transplantation.

### FITC-Labeled Polymeric Micelles and FITC-Albumin

To observe macromolecular behavior *in vivo*, FITC-labeled polymeric micelles (Mw of the block copolymer 15,259) and FITC-albumin (Mw 69,680) (Sigma–Aldrich Japan K.K., Tokyo, Japan) were used. FITC-labeled micelles were synthesized by the Kanagawa Academy of Science and Technology. The characteristics of this polymeric micelle preparation were described in detail elsewhere.[10] In brief, the micelle consists of the poly(ethylene glycol)-*b*-poly (benzyl-L-aspartate) block copolymer, with 16.9% of

block copolymer being labeled by FITC. The diameter of an FITC-micelle measured $48.2 \pm 8.8$ nm.[10] The basic structure of this micelle system was almost the same as that of the previously described micelle-encapsulated doxorubicin.[23] This type of micelles was shown to have circulation stability,[23] and a previous experiment confirmed that the half-life of the present micelle preparation in blood is ~9 h.[10] FITC-albumin consisted of bovine serum albumin, and its FITC content was 12 mol/mol albumin. The radius of gyration of bovine serum albumin is reported to be 3.2 nm.[24] FITC-micelles and FITC-albumin were administered i.v. at doses of 20 and 15 mg/kg, respectively.

### Tumor Vascular Disrupting Agent

In the present study, Cderiv (formerly known as AC7700) was used as the tumor vascular disrupting agent. It was synthesized at Tokyo Kasei Kogyo Co. according to the method of Ohsumi et al.[14] Cderiv had been developed by Ajinomoto Pharmaceutical Research Laboratories,[14] and we demonstrated that it greatly disrupted tumor blood flow.[16–20] Immediately before use, the Cderiv powder was dissolved in 0.9% NaCl solution, to give a final concentration of 10 mg/mL. The solution (10 mg/kg) was injected into the tail vein of rats at a rate of 0.15 mL/min by using an infusion pump. This Cderiv dose did not produce conspicuous side effects, such as body weight loss, anemia, and diarrhea, in our rat model.[16]

### X-Irradiation

To investigate the behavior of polymeric micelles and albumin in irradiated tumors, an X-irradiation generator (MBR-1520R; Hitachi Medical Corp., Tokyo, Japan) was utilized. The method of X-irradiation was previously described in detail.[21]

### Vital Microscopic Observation

Tumor microcirculation in the chamber was transilluminated by a 12-V 100-W halogen lamp and was directly observed with a light microscope (Eclipse E800; Nikon Co., Tokyo, Japan), with 10× ocular (CFI UW; Nikon Co.) and 2–20× objectives (CFI Plan Fluor; Nikon Co.). Microscopic images were recorded by using a closed-circuit video system consisting of a CCD video camera (CS-900; Olympus Co., Tokyo, Japan), TV monitor (PVM-14M4J; Sony Co., Tokyo, Japan), and S-VHS video recorder (SVO-2100; Sony Co.).

### Fluorescence Microscopic Analysis of FITC-Labeled Compounds

For intravital fluorescence microscopy, the light source was a high-pressure mercury lamp (C-SHG1; Nikon Co.). Tumor vessels in the chamber were epi-illuminated and photographed through a 420- to 490-nm primary filter, 505-nm dichroic interference mirror, and 520-nm secondary filter. FITC-labeled compounds were injected into rats as a single i.v. bolus. Microscopic images of extravasation of FITC-labeled compounds were photographed with a silicon-intensified video camera (C2400-08; Hamamatsu Photonics, Hamamatsu, Japan) and were recorded with a video recorder. The slight positional change of the observation area that occurred during the long experiment was adjusted every 3–4 h. Analog images on video tape were converted to digital images by means of a video capture device (PC-MDVD/U2; Buffalo, Inc., Nagoya, Japan). The digital images were recorded on a DVD.

For image analysis, segments of time-lapse images were transferred from the DVD to a computer hard disk (Dimension 9150; Dell Japan, Inc., Kawasaki, Japan). Temporal changes in fluorescence intensity of regions of interest (ROIs) in tissue in the chambers were measured by means of NIH ImageJ (V1.61, http:/rsb.info.nih.gov/nih-image/).[21] For this analysis, images obtained via the 20× objective were used. The labeled fluorescent substances circulated in blood vessels only just after i.v. administration. Therefore, blood vessels and extravascular spaces could easily be distinguished. In the present study, fluorescence intensity in tissues was measured by carefully removing blood vessel areas from the images of the entire tumor tissue.[10] Thus, selected ROIs were distant from the blood vessels. One ROI (10 $\mu m^2$) consisted of 100 pixels, and 5–10 ROIs per chamber were randomly selected for analysis.

### Changes in Extravasation and Retention of Fluorescent Macromolecules Caused by Cderiv

Our preliminary experiment showed that damage of LY80 tumor tissues became prominent 24 h after Cderiv administration and that tumor blood flow recovered and tumors began to regrow 72 h later, when the Cderiv effect declined to insufficient levels. Therefore, to analyze changes in extravasation and retention of fluorescent macromolecules caused by vascular disruption, Cderiv (10 mg/kg) was administered i.v. 24 or 72 h before i.v. administration of FITC-micelles or FITC-albumin. The changes in intratumor fluorescence intensity over time for the groups treated with Cderiv and the controls were compared.

### Changes in Extravasation and Retention of Fluorescent Macromolecules Caused by X-Irradiation

Another preliminary experiment showed prominent LY80 tumor tissue damage 72 h after 10-Gy X-irradiation, after which tumor volume began to decrease. Therefore, tumors growing in transparent chambers were irradiated 72 h before i.v. administration of FITC-micelles or FITC-albumin. The changes in extravasation and retention of fluorescent macromolecules over time that were caused by

X-irradiation were measured. In this experiment, washout of FITC-albumin from tissues was evaluated by measuring the half-life ($t_{1/2}$) of fluorescence intensity.

### Identification of Necrotic Areas in Tumors

Part of the tumor tissue in transparent chambers became necrotic after i.v. administration of Cderiv or X-irradiation. In the case of Cderiv, tumor blood flow was greatly disrupted, and the necrotic areas changed color. In the present study, a necrotic area was defined as a tumor region in a transparent chamber in which circulation completely stopped for more than 24 h and thus the color of the tissue changed to gray.[10] In the case of X-irradiation, although tumor blood flow increased somewhat, many tumor cells became gray. That such a region was necrotic was histologically confirmed.

Histological sections were prepared as follows. One rat with a transparent chamber was sacrificed via deep ether anesthesia at the end of the experiment. The glass window of one side of the chamber was gently removed; 15% formalin solution was dropped directly on the tissue (~150 μm thick); and the thin tissue was fixed, processed, and embedded in paraffin. Sections (4 μm thick) were cut parallel to the surface of the membrane tissue within the transparent chamber and were stained with hematoxylin and eosin.

### Statistics

All results are expressed as means ± SD. The statistical significance of the difference among groups for the various conditions for extravasation of FITC-labeled compounds was evaluated via repeated-measures ANOVA. The significance of the difference in half-life of FITC-albumin between irradiated and nonirradiated tumors was evaluated via unpaired two-group $t$ tests. $p$ values of 0.05 or lower were considered significant.

## RESULTS

### Effects of Cderiv Pretreatment on Extravasation and Retention of FITC-Micelles in Microtumors

Figure 1 shows a representative vital microscopic finding of FITC-micelle accumulation in a necrotic

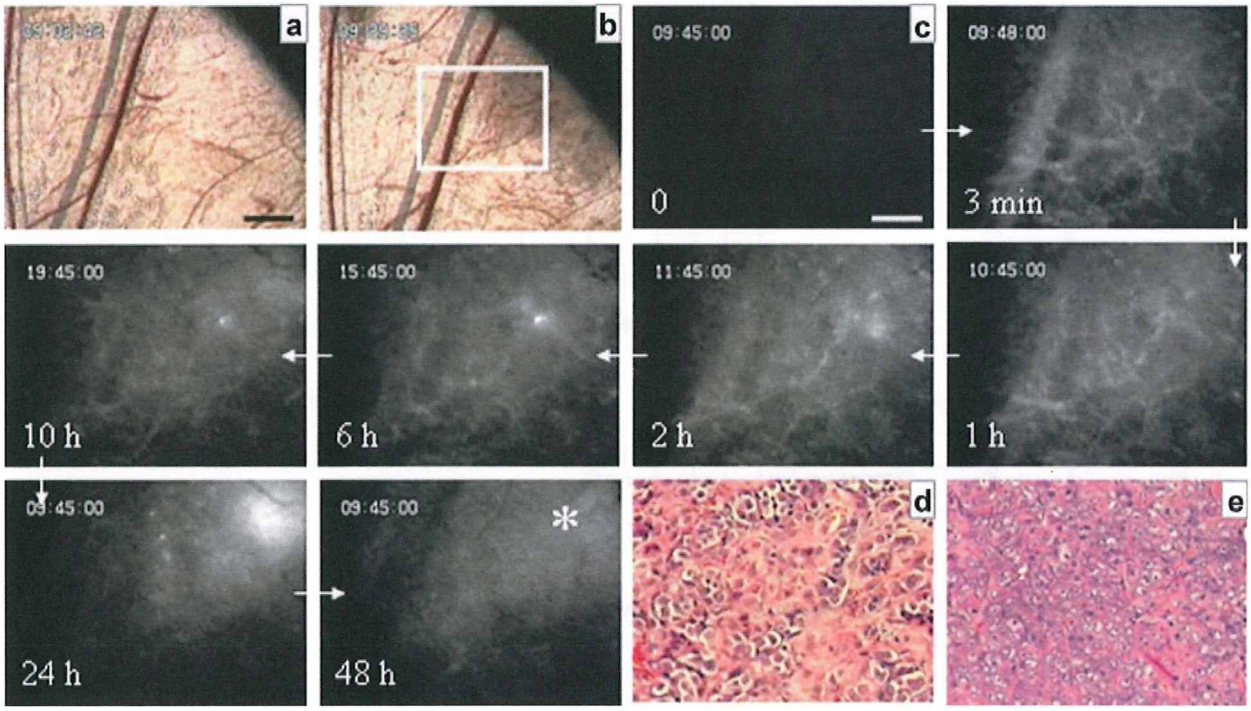


**Figure 1.** Accumulation of FITC-micelles in necrotic LY80 tumor tissue after Cderiv pretreatment. (a) Vital microscopy before Cderiv administration. (b) Vital microscopy 24 h after i.v. administration of Cderiv. The white frame is the area shown in the fluorescence images. The gray region in the frame is tumor tissue damage by Cderiv. (c) Fluorescence microscopy. The time after FITC-micelle (20 mg/kg) administration appears at the lower left in each panel. Arrows indicate the direction of time. Scale bars: (a) 200 μm; (c) 100 μm. (d) Histology of the area indicated by the asterisk. (e) Histology of nontreated tumor in the transparent chamber. Hematoxylin and eosin staining. The area of FITC-micelle distribution coincides with the gray region (necrotic area).

part of the tumor; Cderiv (10 mg/kg) had been administered 1 day earlier. The area that had changed to gray (seen in the white frame in Fig. 1b) is tumor tissue damaged by Cderiv. FITC-micelles extravasated into tumor tissues as early as 3 min after i.v. administration (Fig. 1c). Permeability of vessels in the microtumor that survived for 24 h after Cderiv pretreatment was markedly enhanced. The localization of FITC-micelles coincided with the necrotic area, and these micelles were seen in the area even 48 h later (Fig. 1, asterisk). Figure 1d shows the histology of the gray region affected by Cderiv. This region evidenced prominent granulation compared with the control (Fig. 1e).

Figure 2A presents typical extravasation and retention of FITC-micelles in tumor tissue when FITC-micelles were administered i.v. 3 days after Cderiv (10 mg/kg, i.v.). Figure 2B shows the difference in time changes of fluorescence intensity between the group pretreated with Cderiv and the control group. Extravasation from tumor vessels that survived Cderiv pretreatment and had restored blood

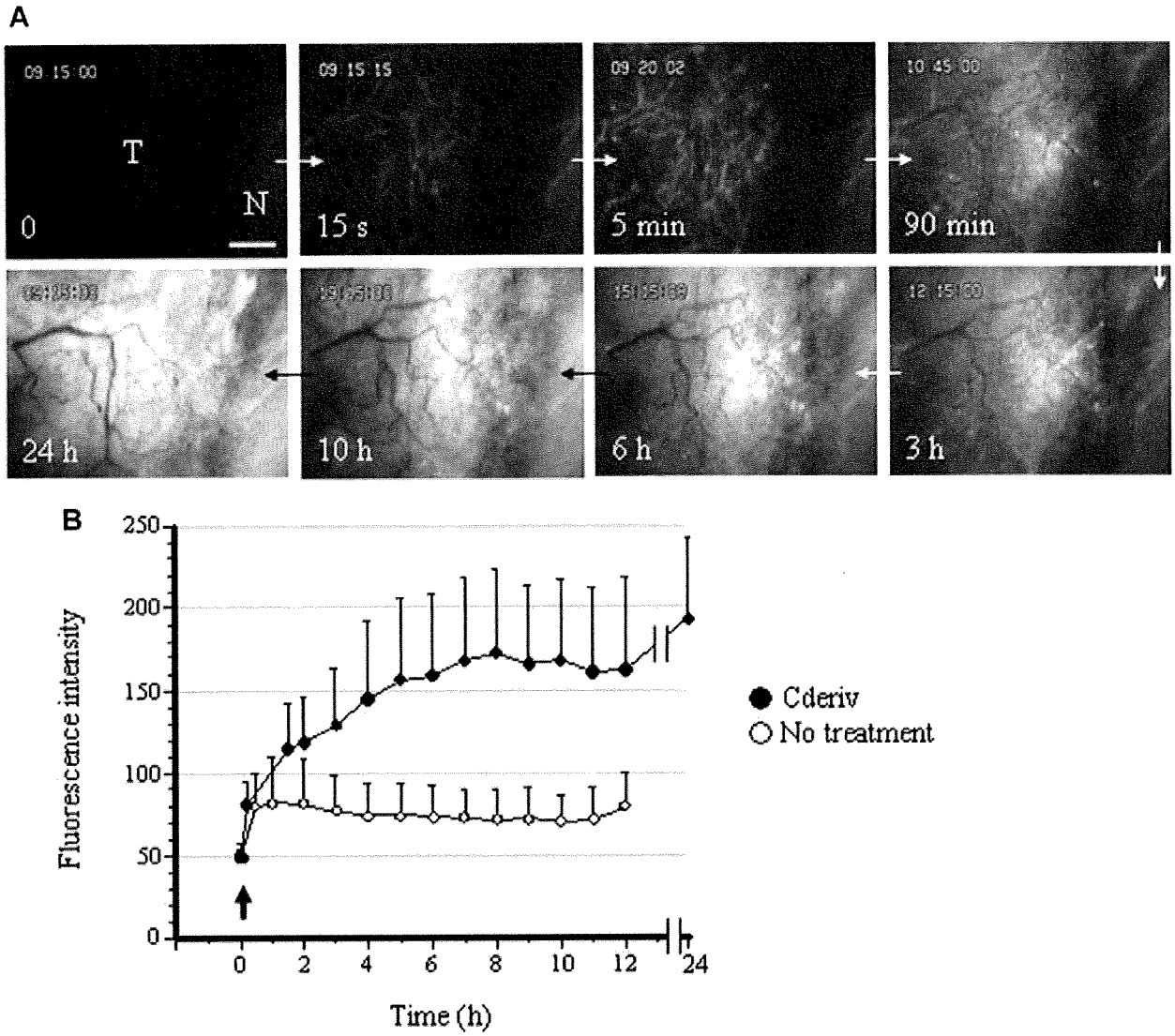


**Figure 2.** Extravasation and retention of FITC-micelles in LY80 microtumors that were pretreated with Cderiv. (A) Typical extravasation and retention of FITC-micelles in a microtumor treated with Cderiv (10 mg/kg, i.v.) 3 days previously. The time after FITC-micelle (20 mg/kg) administration appears at the lower left in each panel. Arrows indicate the direction of time. T, tumor; N, necrosis. Scale bar: 200 μm. (B) Time course of fluorescence intensity of FITC-micelles in tumor tissue treated with Cderiv ($n = 10$) and nontreated tumor tissue ($n = 25$). Cderiv was given i.v. 3 days before FITC-micelles. The micelle solution was administered i.v. at 0 h (arrow). Maximum fluorescence intensity was 255.

flow was markedly enhanced compared with extravasation from intact vessels of microtumors ($p < 0.0001$). A high concentration of extravasated micelles was seen, especially in necrotic areas with microcirculatory dysfunction, and the high concentration continued even to 24 h (Fig. 2).

### Extravasation and Retention of FITC-Micelles in a Microtumor Receiving 10 Gy X-Irradiation

Figure 3 presents typical extravasation and retention of FITC-micelles in a microtumor that had received 10 Gy X-irradiation 3 days before. A considerable amount of FITC-micelles extravasated into tumor tissue 5 min after i.v. administration. This result means that X-irradiation markedly enhanced the vascular permeability of the microtumor. Although X-irradiation caused the tumor tissue to collapse (Fig. 3d), extravasated micelles did not remain in the tumor. This finding differed from that for Cderiv pretreatment.

### Extravasation and Retention of FITC-Albumin in Microtumors

Figure 4A shows typical extravasation and retention of FITC-albumin in a microtumor. The vascular network had already been established in a microtumor smaller than 500 μm in diameter (Fig. 4A-c). However, no giant capillaries, with abnormal vascular dilatation and hyperpermeability, were observed. Significantly less extravasation of FITC-albumin was observed from the vascular network of microtumors than from vessels at the interface between normal and tumor tissues ($p < 0.0001$) (Fig. 4B). Extravasated FITC-albumin in and around microtumors was gradually flushed out and never accumulated there.

### Extravasation and Retention of FITC-Albumin Before and After Administration of Cderiv in Microtumors

Figure 5A illustrates extravasation and retention of FITC-albumin in a microtumor before Cderiv pretreatment. Figure 5B shows the change in extravasation and retention in the same area 1 day after i.v. administration of 10 mg/kg Cderiv. Less extravasation of FITC-albumin was noted from vessels in the microtumor than from vessels outside the microtumor.

When FITC-albumin was again administered i.v. after Cderiv pretreatment, it accumulated predominantly in the necrotic area (gray region in Fig. 5B-a) of the tumor. FITC-albumin remained in the necrotic region (Fig. 5C-c-1) even 31 h after administration but was flushed out of viable regions (Fig. 5C-c-2).

### Extravasation and Retention of FITC-Albumin in a Microtumor Receiving 10 Gy X-Irradiation

Figure 6 shows typical extravasation and retention of FITC-albumin in a microtumor that had received 10 Gy X-irradiation 3 days before. X-irradiation caused all tumor vessels to narrow, and the structure of the tumor vascular network became less complex. Although tumor vessels looked as if they had normalized morphologically, vascular permeability to FITC-albumin was rather enhanced. As shown in Figure 3d, prominent granulation was observed in the LY80 tumor tissue 3 days after X-irradiation.

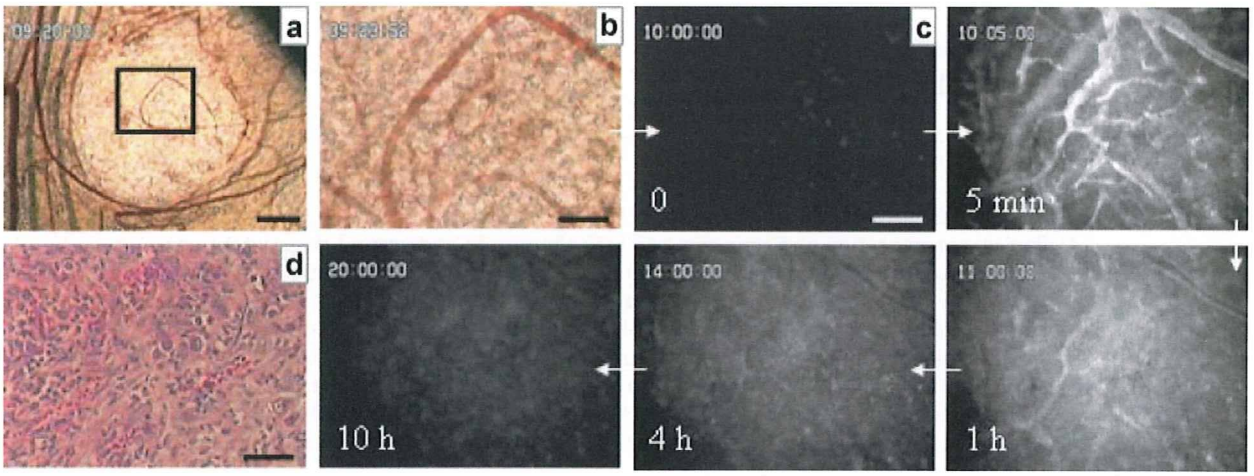


**Figure 3.** Extravasation and retention of FITC-micelles in an LY80 microtumor receiving X-irradiation. (a) Vital microscopy of a microtumor that had received 10 Gy 72 h before. The black frame is the area shown in the fluorescence images. (b) High-power magnification of the area in the black frame in a. (c) Fluorescence microscopy. The time after FITC-micelle (20 mg/kg) administration appears at the lower left in each panel. Arrows indicate the direction of time. (d) Histology of tumor tissue at 72 h after 10 Gy X-irradiation. Hematoxylin and eosin staining. Scale bars: (a) 200 μm; (b and c) 100 μm; (d) 50 μm.

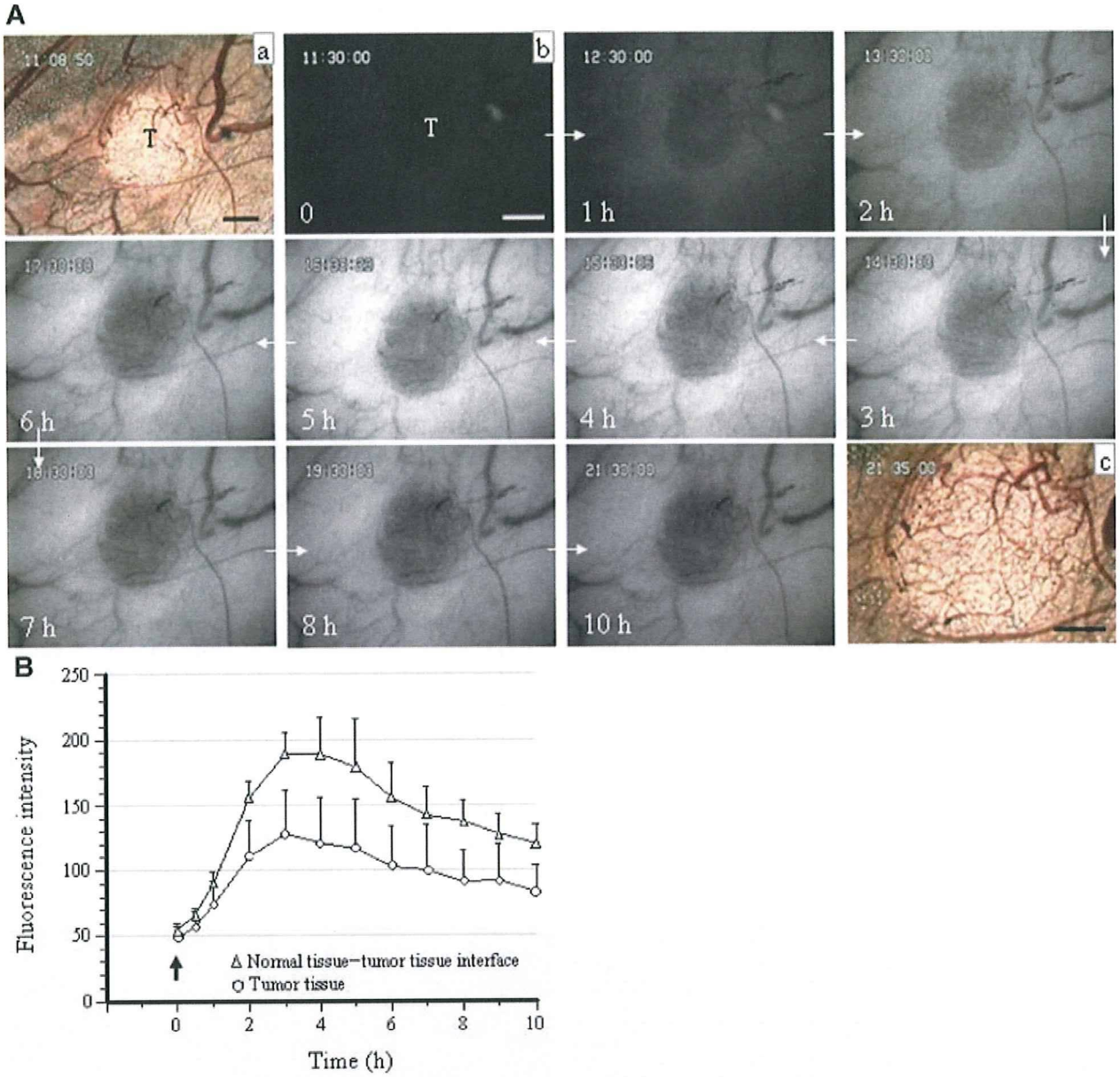


**Figure 4.** Extravasation and retention of FITC-albumin in LY80 microtumors. (A) Typical extravasation and retention of FITC-albumin in and around the microtumor. (a) Vital microscopy. T, microtumor. (b) Fluorescence microscopy. The time after FITC-albumin (15 mg/kg) administration appears at the lower left in each panel. Arrows indicate the direction of time. (c) Vital microscopy 10 h later, showing that a microtumor <500 μm in diameter establishes its own microvascular network. Scale bars: (a and b) 200 μm; (c) 100 μm. (B) Time course of fluorescence intensity of FITC-albumin in tumor tissue ($n = 18$) and at the interface between normal tissue and tumor tissue ($n = 10$). The albumin solution was administered i.v. at 0 h (arrow). Maximum fluorescence intensity was 255.

However, the microcirculation in these tumors functioned quite well. Unlike the situation with Cderiv, extravasated FITC-albumin did not accumulate in necrotic regions and was gradually flushed out of the region.

Figure 7 shows the time course of fluorescence intensity of intratumor FITC-albumin in the Cderiv, X-irradiation, and untreated control groups. Extravasation of FITC-albumin from vessels in tumors that had received 10 Gy X-irradiation was markedly enhanced compared with that from vessels in untreated tumors ($p < 0.0001$). However, the half-life of FITC-albumin in X-irradiated tissue was significantly shortened, from $10.0 \pm 2.1$ h ($n = 17$) to $5.2 \pm 0.4$ h ($n = 10$) ($p < 0.0001$), which shows that washout was accelerated and it became difficult for

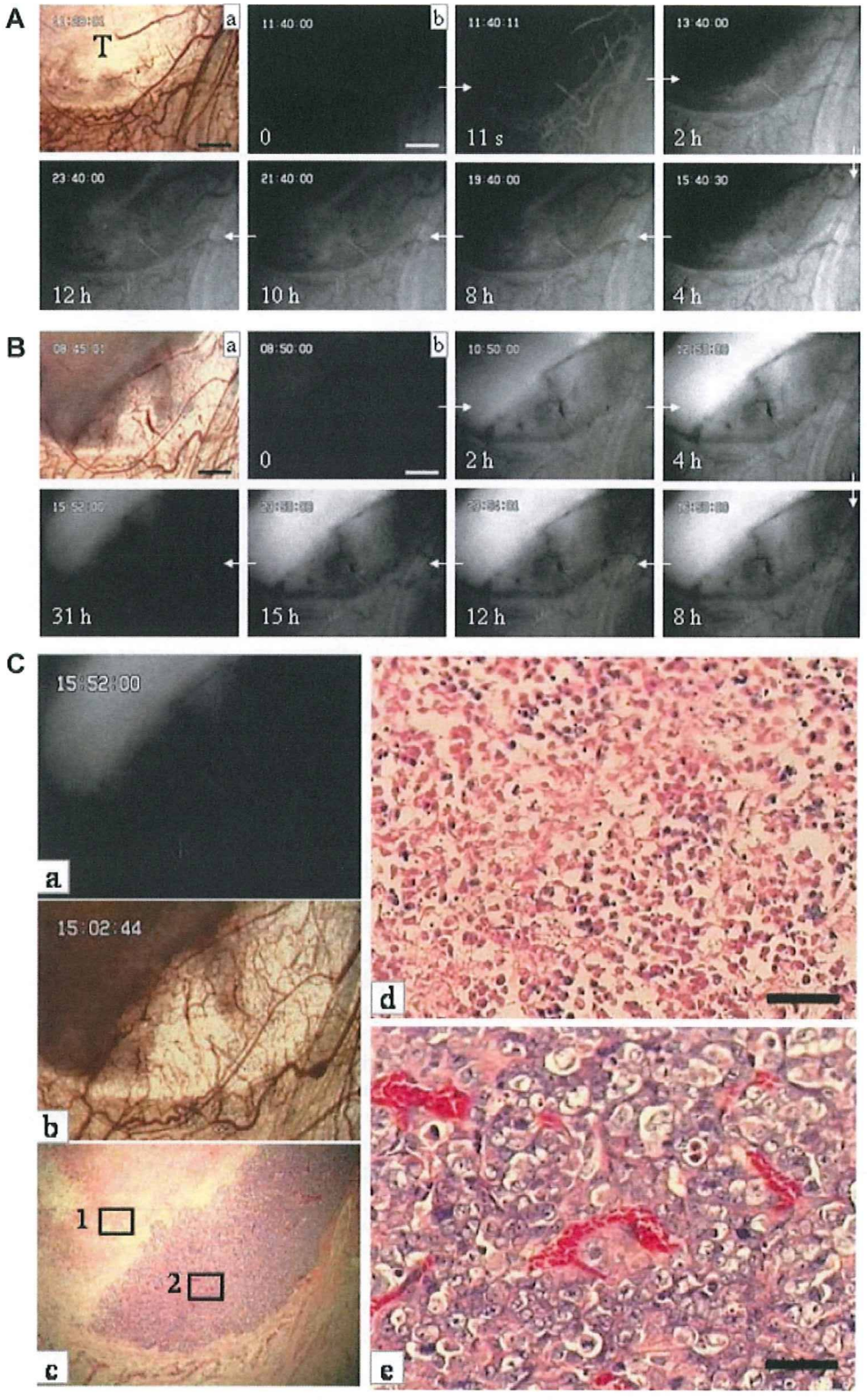
A
T
a
11:40:00
b
0
11:40:11
11 s
13:40:00
2 h
23:40:00
12 h
21:40:00
10 h
19:40:00
8 h
15:40:30
4 h
B
a
08:50:00
b
0
10:50:00
2 h
4 h
31 h
15 h
12 h
8 h
C
15:52:00
a
15:02:44
b
1
2
c
d
e

**Figure 5.**

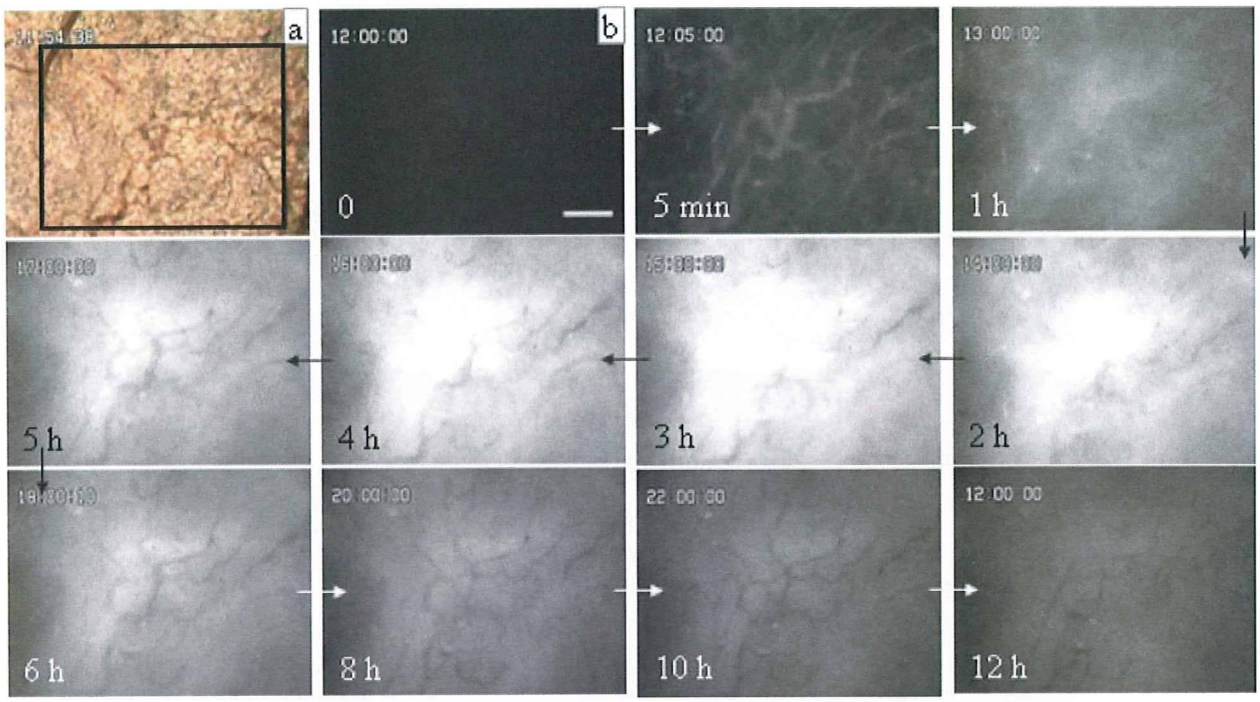


**Figure 6.** Extravasation and retention of FITC-albumin in LY80 tumors receiving X-irradiation. (a) Vital microscopy of a tumor that had received 10 Gy 72 h previously. The black frame is the area shown in the fluorescence images. (b) Fluorescence microscopy. The time after FITC-albumin (15 mg/kg) administration appears at the lower left in each panel. Arrows indicate the direction of time. Scale bar: 100 μm.

FITC-albumin to remain in the tumor. Extravasation from tumor vessels that survived after Cderiv treatment and had restored tumor blood flow was also markedly enhanced compared with that from untreated tumor vessels ($p < 0.0001$). However, unlike the situation with X-irradiation, FITC-albumin was not flushed out of tumors and remained there at a high concentration even 12 h after administration.

## DISCUSSION

To date, many reports have shown that tumor vessels have higher permeability than normal blood vessels. To explain this feature, researchers have pointed to the following characteristics of tumor vessels: (i) tumor vessels usually have wider intercellular junctions than normal vessels,[25] (ii) many tumor vessels have fenestrated structures,[26] (iii) endothelial cells of tumor vessels have more vesiculo-vacuolar organelles than those of normal vessels,[27] and (iv) some tumor vessels lack endothelial cells.[28] These characteristics were identified by studying vessels in advanced tumors, whose vessels differ significantly from normal blood vessels. In general, however, vessels with different morphologies and functions exist in a tumor because tumor vessels change markedly during tumor growth.[29,30] Among these

**Figure 5.** Changes in extravasation and retention of FITC-albumin in an LY80 tumor before and after Cderiv pretreatment. (A) Before Cderiv pretreatment. (a) Vital microscopy. T, tumor. (b) Fluorescence microscopy. The time after FITC-albumin (15 mg/kg) administration appears at the lower left in each panel. Arrows indicate the direction of time. Scale bars: (a) 250 μm; (b) 200 μm. (B) At 24 h after Cderiv (10 mg/kg) pretreatment. The observation area is the same as that in A. (a) Vital microscopy. The gray region is the area of necrosis caused by Cderiv. (b) Fluorescence microscopy. The time after FITC-albumin (15 mg/kg) readministration appears at the lower left in each panel. Arrows indicate the direction of time. Scale bars: (a) 250 μm; (b) 200 μm. (C) Detailed study of the area shown in B. (a) Fluorescence microscopy. (b) Vital microscopy. The observation area is the same as that in a. (c) Histology of the area shown in b. (d) High-power magnification of the area in the frame 1 in c. (e) High-power magnification of the area in the frame 2 in c. Scale bars: 50 μm. (c–e) Hematoxylin and eosin staining. Note that FITC-albumin accumulated in the necrotic area.

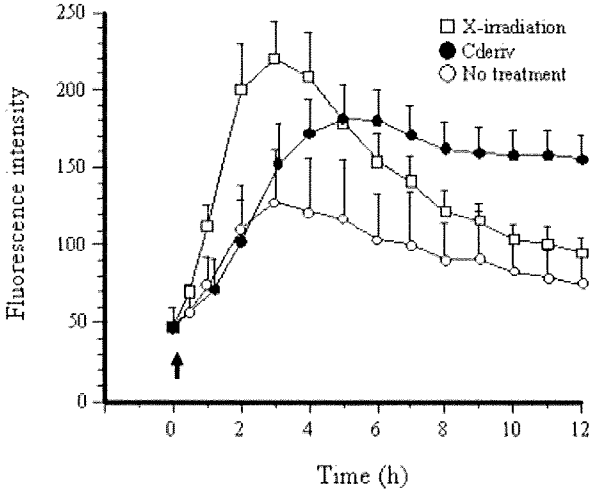


**Figure 7.** Time course of fluorescence intensity of FITC-albumin in LY80 tumors that had received Cderiv (10 mg/kg; $n = 10$), X-irradiation (10 Gy; $n = 10$), or no treatment ($n = 18$). Cderiv or X-irradiation was given 3 days before i.v. administration of FITC-albumin. FITC-albumin was given i.v. at 0 h (arrow). Maximum fluorescence intensity was 255.

studies of tumor vessels, very few reports have appeared about the function of vessels of microtumors. However, whether those characteristics of tumor vessels just outlined above apply to blood vessels of microtumors must be clarified.

Recently, using a vital microscopic observation system together with a transparent chamber setup, we investigated the function of vessels in microtumors.[10] Results showed that the accepted belief [11–13] that tumor vessels have higher permeability than normal vessels is not always the case. For extravasation of our polymeric micelles at least, the function of vessels in microtumors was rather similar to that of normal blood vessels. Although polymeric micelles readily leaked from vessels in advanced tumors, their extravasation from the vascular network of microtumors was negligible, and micelles never accumulated in such microtumors.[10] Vital microscopic analysis with albumin in the present study showed similar results. That is, the EPR effect did not occur in microtumors. Despite the great difference in the molecular sizes of polymeric micelles and albumin, both substances behaved quite similarly in microtumors. Both distribution and washout were markedly influenced by tumor perfusion. These results agree with the belief that the main driving force of macromolecular movement is convection rather than diffusion.

The present study found that microtumor vessels that survived after treatment with the vascular disrupting agent Cderiv and had restored blood flow became quite leaky. Extravasation of macromolecules from such tumor vessels was markedly enhanced not only in advanced tumors but also in microtumors. Polymeric micelles and albumin that extravasated after i.v. administration accumulated in necrotic areas of microtumors caused by Cderiv. That is, pretreatment with Cderiv resulted in the occurrence of the EPR effect in microtumors. This finding means that the therapeutic effectiveness of anticancer drug-incorporating micelles was extended to micrometastatic foci. Kano et al.[31] reported that transforming growth factor-β type I receptor inhibitor enhanced the EPR effect in intractable solid tumors. However, this study did not address whether the inhibitor would enhance the EPR effect in microtumors.

The reason why early-stage tumor vessels became leaky after Cderiv pretreatment is not yet clear. Tozer et al.[32] reported that combretastatin A-4 phosphate enhanced tumor vascular permeability. We could not evaluate the direct effect caused by Cderiv on tumor vascular permeability, however, because tumor blood flow began to decrease shortly after Cderiv administration and stopped completely within 30 min. Nevertheless, our previous study showed that tumor interstitial fluid pressure markedly decreased just after Cderiv administration and did not recover to the original level even after 6 h.[17] This finding strongly suggests that tumor vascular permeability was not enhanced, at least shortly after administration of Cderiv. The difference in activity of combretastatin A-4 phosphate and Cderiv is probably related to a difference in the degree of tumor blood flow interruption caused by each drug. In the case of Cderiv, some unknown factor may cause tumor vascular structure to collapse during the tumor blood flow halt. We are now investigating the reason for this effect.

We also found, when tumors received 10 Gy X-irradiation before i.v. administration of FITC-micelles, that extravasation was markedly enhanced but that the extravasated micelles did not remain in the tumor tissues. Also, like FITC-micelles, FITC-albumin did not accumulate in tumors that had received 10 Gy X-irradiation; this result is clearly different from the case for pretreatment with Cderiv. Histological examination showed many areas of granulation within tumors 3 days after 10 Gy X-irradiation. However, the fact that macromolecules did not accumulate there indicates that enhanced extravasation of macromolecules does not always lead to accumulation of macromolecules. Intratumor accumulation of macromolecules needs the drainage system to stop functioning, as Maeda emphasized.[1,12]

The reason that macromolecules were washed out of tumors that had received 10 Gy X-irradiation is probably related to improved tumor microcirculation, because the increased tumor blood flow reached a maximum 3 days after 10 Gy X-irradiation.[21] Although tissue degradation seems to be essential

for the EPR effect to occur, that such tissues have dysfunctional microcirculation may be sufficient.

Liposomes, one type of nanocarrier, have been reported to accumulate in high concentrations in tumors that received photodynamic therapy.[33–35] Photodynamic therapy induces enhanced permeability and tumor microcirculatory dysfunction. Although we have not as yet confirmed this possibility, vascular disrupting agents and photodynamic therapy may have similar effects against tumor vessels.

In conclusion, the EPR effect operates primarily in tumors that include necrotic areas. This effect does not occur in microtumors because tumors <3 mm in diameter usually have no necrotic areas. In the present study, we demonstrated that induction of necrosis in a tumor area would lead to the occurrence of the EPR effect, even in microtumors. This discovery is a breakthrough for retaining nanomedicines in microtumors for a long period. The procedure described in the present study may thus become a promising means for attacking micrometastatic foci.

## ACKNOWLEDGMENTS

We thank Ms. H. Oikawa for expert technical assistance. This work was supported by grant H18-nano-004 for Scientific Research from the Ministry of Health, Labor and Welfare, Japan, by grant 19591449 for Scientific Research from the Ministry of Education, Science, Sports and Culture, Japan (K.H.), by JST, CERST, and by the Program for Promoting the Establishment of Strategic Research Centers, Special Coordination Funds for Promoting Science and Technology, the Ministry of Education, Culture, Sports, Science, and Technology, Japan (M.N., K.S., and M.Y.).

## REFERENCES

1. Maeda H. 1994. Polymer conjugated macromolecular drugs for tumor-specific targeting. In: Domb AJ, editor. Polymeric site-specific pharmacotherapy. New York: Wiley. pp. 95–116.
2. Yokoyama M, Opanasopit P, Kawano K, Okano T, Maitani Y. 2004. Polymer design and incorporation methods for polymeric micelle carrier system containing water-insoluble anti-cancer agent camptothecin. J Drug Target 12:373–384.
3. Hamaguchi T, Matsumura Y, Suzuki M, Shimizu K, Goda R, Nakamura I, Nakatomi I, Yokoyama M, Kataoka K, Kakizoe T. 2005. NK105, a paclitaxel-incorporating micellar nanoparticle formulation, can extend in vivo antitumor activity and reduce the neurotoxicity of paclitaxel. Br J Cancer 92:1240–1246.
4. Duncan R. 2006. Polymer conjugates as anticancer nanomedicines. Nat Rev Cancer 6:688–701.
5. Koizumi F, Kitagawa M, Negishi T, Onda T, Matsumoto S, Hamaguchi T, Matsumura Y. 2006. Novel SN-38-incorporating polymeric micelles, NK012, eradicate vascular endothelial growth factor-secreting bulky tumors. Cancer Res 66:10048–10056.
6. Cabral H, Nishiyama N, Kataoka K. 2007. Optimization of (1,2-diamino- cyclohexane)platinum (II)-loaded polymeric micelles directed to improved tumor targeting and enhanced antitumor activity. J Control Release 121:146–155.
7. Matsumura Y. 2008. Poly (amino acid) micelle nanocarriers in preclinical and clinical studies. Adv Drug Deliv Rev 60:899–914.
8. Lammers T, Hennink WE, Storm G. 2008. Tumour-targeted nanomedicines: Principles and practice. Br J Cancer 99:392–397.
9. Watanabe M, Kawano K, Toma K, Hattori Y, Maitani Y. 2008. In vivo antitumor activity of camptothecin incorporated in liposomes formulated with an artificial lipid and human serum albumin. J Control Release 127:231–238.
10. Hori K, Nishihara M, Yokoyama M. 2009. Vital microscopic analysis of polymeric micelle extravasation from tumor vessels: Macromolecular delivery according to tumor vascular growth stage. J Pharm Sci [ Published Online: 18 June 2009 [Epub ahead of print], 10.1002/jps.21848. ]
11. Matsumura Y, Maeda H. 1986. A new concept for macromolecular therapeutics in cancer chemotherapy: Mechanism of tumoritropic accumulation of proteins and the antitumor agent smancs. Cancer Res 46:6387–6392.
12. Maeda H, Wu J, Sawa T, Matsumura Y, Hori K. 2000. Tumor vascular permeability and EPR effect for macromolecular therapeutics. J Control Release 65:271–284.
13. Greish K. 2007. Enhanced permeability and retention of macromolecular drugs in solid tumors: A royal gate for targeted anticancer nanomedicines. J Drug Target 15:457–464.
14. Ohsumi K, Nakagawa R, Fukuda Y, Hatanaka T, Morinaga Y, Nihei Y, Ohishi K, Suga Y, Akiyama Y, Tsuji T. 1998. Novel combretastatin analogues effective against murine solid tumors: Design and structure-activity relationships. J Med Chem 41:3022–3032.
15. Nihei Y, Suga Y, Morinaga Y, Ohishi K, Okano A, Ohsumi K, Hatanaka T, Nakagawa R, Tsuji T, Akiyama Y, Saito S, Hori K, Sato Y, Tsuruo T. 1999. A novel combretastatin A-4 derivative, AC-7700, shows marked antitumor activity against advanced solid tumors and orthotopically transplanted tumors. Jpn J Cancer Res 90:1016–1025.
16. Hori K, Saito S, Nihei Y, Suzuki M, Sato Y. 1999. Antitumor effects due to irreversible stoppage of tumor tissue blood flow: Evaluation of a novel combretastatin A-4 derivative, AC7700. Jpn J Cancer Res 90:1026–1038.
17. Hori K, Saito S. 2003. Microvascular mechanisms by which the combretastatin A-4 derivative AC7700 (AVE8062) induces tumour blood flow stasis. Br J Cancer 89:1334–1344.
18. Hori K. 2005. Cancer therapy by means of irreversible tumor blood flow stasis: Starvation tactics against solid tumors. Gene Ther Mol Biol 9:203–216.
19. Hori K, Saito S, Sato Y, Kubota K. 2001. Stoppage of blood flow in 3-methylcholanthrene-induced autochthonous primary tumor due to a novel combretastatin A-4 derivative, AC7700, and its antitumor effect. Med Sci Monit 7:26–33.
20. Hori K, Saito S, Kubota K. 2002. A novel combretastatin A-4 derivative, AC7700, strongly stanches tumour blood flow and inhibits growth of tumours developing in various tissues and organs. Br J Cancer 86:1604–1614.
21. Hori K, Furumoto S, Kubota K. 2008. Tumor blood flow interruption after radiotherapy strongly inhibits tumor regrowth. Cancer Sci 99:1485–1491.
22. Hori K, Suzuki M, Tanda S, Saito S. 1990. In vivo analysis of tumor vascularization in the rat. Jpn J Cancer Res 81:279–288.

23. Yokoyama M, Okano T, Sakurai Y, Fukushima S, Okamoto K, Kataoka K. 1999. Selective delivery of adriamycin to a solid tumor using a polymeric micelle carrier system. J Drug Target 7:171–186.
24. Murthy NS, Knox JR. 2004. Hydration of proteins: SAXS study of native and methoxy polyethyleneglycol (mPEG)-modified L-asparaginase and bovine serum albumin in mPEG solutions. Biopolymers 74:457–466.
25. Long DM. 1970. Capillary ultrastructure and the blood-brain barrier in human malignant brain tumors. J Neurosurg 32: 127–144.
26. Roberts WG, Palade GE. 1997. Neovasculature induced by vascular endothelial growth factor is fenestrated. Cancer Res 57:765–772.
27. Feng D, Nagy JA, Hipp J, Dvorak HF, Dvorak AM. 1996. Vesiculo-vacuolar organelles and the regulation of venule permeability to macromolecules by vascular permeability factor, histamine, and serotonin. J Exp Med 183:1981–1986.
28. Hashizume H, Baluk P, Morikawa S, McLean JW, Thurston G, Roberge S, Jain RK, McDonald DM. 2000. Openings between defective endothelial cells explain tumor vessel leakiness. Am J Pathol 156:1363–1380.
29. Yamaura H, Sato H. 1974. Quantitative studies on the developing vascular system of rat hepatoma. J Natl Cancer Inst 53:1229–1240.
30. Warren BA. 1979. The vascular morphology of tumors. In: Peterson HI, editor. Tumor blood circulation. Boca Raton, Florida: CRC Press. pp. 1–47.
31. Kano MR, Bae Y, Iwata C, Morishita Y, Yashiro M, Oka M, Fujii T, Komuro A, Kiyono K, Kaminishi M, Hirakawa K, Ouchi Y, Nishiyama N, Kataoka K, Miyazono K. 2007. Improvement of cancer-targeting therapy, using nanocarriers for intractable solid tumors by inhibition of TGF-β signaling. Proc Natl Acad Sci USA 104:3460–3465.
32. Tozer GM, Prise VE, Wilson J, Cemazar M, Shan S, Dewhirst MW, Barber PR, Vojnovic B, Chaplin DJ. 2001. Mechanisms associated with tumor vascular shut-down induced by combretastatin A-4 phosphate: Intravital microscopy and measurement of vascular permeability. Cancer Res 61:6413–6422.
33. Chen B, Pogue BW, Luna JM, Hardman RL, Hoopes PJ, Hasan T. 2006. Tumor vascular permeabilization by vascular-targeting photosensitization: Effects, mechanism, and therapeutic implications. Clin Cancer Res 12:917–923.
34. He C, Agharkar P, Chen B. 2008. Intravital microscopic analysis of vascular perfusion and macromolecule extravasation after photodynamic vascular targeting therapy. Pharm Res 25: 1873–1880.
35. Snyder JW, Greco WR, Bellnier DA, Vaughan L, Henderson BW. 2003. Photodynamic therapy: A means to enhanced drug delivery to tumors. Cancer Res 63:8126–8131.

# インテリアCTにおける画像再構成法の提案

筑波大学大学院 システム情報工学研究科コンピュータサイエンス専攻
工藤博幸／イサム ラシド

## はじめに

CT装置の被ばく量を低減する手法には各社工夫を施しており、たとえば①線量を落として撮影した画像を非線形フィルタ処理、②対象物の形状に応じてX線管電圧を変調して雑音の角度依存性をなくすTube Current Modulation、③心臓撮影において時相が合った時点でのみX線管のスイッチをonにする、などの手法が、最先端の装置には導入されている。これらの手法により、ある程度の被ばく量低減は実現できるが、CTイメージングの原理から考えて最も自然で有効な被ばく量低減の手法は、必要のない無駄なX線照射をやめX線を検査の目的とする関心領域（ROI：Region of Interest）だけに照射する手法である。この発想に基づき、筆者らは以下に述べるインテリア（Interior）CTとよばれる新しいCT装置の構成方式を提案した[1,2]。

CTイメージングの多くの状況において、対象物内の小さなROIだけの画像が欲しい場合が生じる。たとえば、心臓病や乳癌の診断では、心臓や乳房を含む小さなROIの画像だけがあれば十分である。現在のCT装置の構成方式やデータ収集法は、このようなROIだけの画像で十分な場合でも、ROIを含む断面を完全に覆うX線ビームを照射して『(ROIのみではなく）対象物断面を通過するすべての直線上の』投影データを測定するものになっている。しかし、直感的にはROIを通過しない直線上の投影データはROIの情報をまったく含んでいないため、不必要なことが予想される。そこで、図1に示すようにROIだけにX線を照射して『ROIを通過する（すべての）直線上の』投影データのみを測定する新しいCT装置の構成方式がインテリアCTである。

インテリアCTの長所や理論的背景については、本誌にすでに2つの論文を執筆したが、ページ数の制約から、インテリアCTにおいて投影データから画像を生成するために必要となる画像再構成法については十分な説明ができなかった[1,2]。そこで、本論文ではインテリアCTを研究開発したい技術者や研究者向けに、筆者らの原著論文で提案されている画像再構成法について解説する[3~9]。ぜひ文献1、2と合わせて読んでいただきたい。

## インテリアCTにおける画像再構成の一意性と安定性

インテリアCTではROIを通過しない直線上の投影データは測定されないため、Interior問題とよばれる一部が欠損した不完全投影データから画像再構成を行う手法が必要となる[3~7]。正確に定義を述べると、Interior問題とは以下に述べる設定の問題である。図2aに示すように対象物$f(x,y)$と画像化対象である凸形状のROI$S$を考える。そして、直線がROI$S$を通過する投影データ$p(r,\phi)$（$r$は動径、$\phi$は角度）のみが測定可能であるとする。ただし、簡単のため平行ビームによる投影データ収集を想定している。この場合、直線がROI$S$を通過しない$p(r,\phi)$は測定されないため、各角度$\phi$の投影データは左右がトランケーションされることになる。このようなトランケーションされた投影データから$f(x,y)$をROI$S$で厳密に再構成する問題がInterior問題である。残念ながらInterior問題の解は測定した投影データ$p(r,\phi)$の情報のみでは一意に定まらないことが知られており、解の一意性と安定性を保証して数

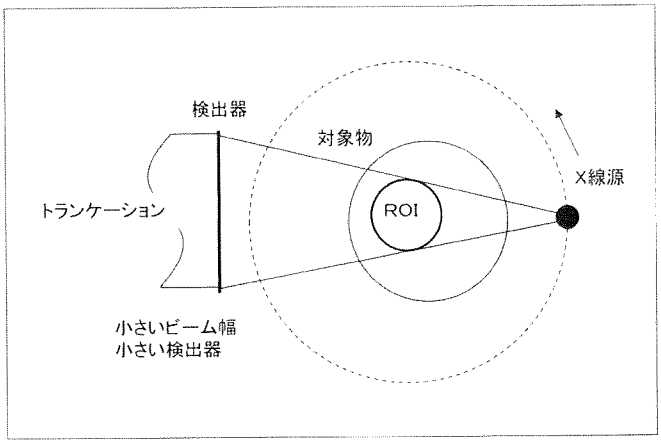

図1　インテリアCTの原理

学的に厳密な再構成を行うには、対象物$f(x,y)$に関する先見的知識（$f(x,y)$の値がROI$S$の内部の指定された領域$B$で事前に既知であること）が必要となる。

2008年現在において、解の一意性と安定性の両方が保証されるROI$S$の形状・配置と先見的知識の組み合わせで最も一般性があり強い結果は、Kudoらの論文に述べられているもので、以下の2つの結果に要約される[4-6]。

［結果1］ROI$S$は対象物の内部に完全に含まれ、先見的知識として$S$の内部にある任意の領域$B$において画像$f(x,y)$の値が既知であると仮定する。ただし、$B$はいくら小さな領域であってもよい（一点のみではだめ）。このとき、投影データ$p(r,\phi)$の情報と先見的知識から、$f(x,y)$はROI$S$で一意に定まり、逆変換は安定である。

［結果2］結果2は結果1を先見的知識が大きい場合に拡張したものである。ROI$S$は対象物の内部に完全に含まれると仮定する。投影データ$p(r,\phi)$は、$S$の内部にある領域$H$（複数の領域のunionでも可）を通過するすべての直線について測定されていると仮定する。また、先見的知識として$S$の内部にある領域$K$において画像$f(x,y)$の値が既知であると仮定する。このとき、3領域$S$、$H$、$K$が以下の2つの条件を満足すれば、投影データ$p(r,\phi)$の情報と先見的知識から、$f(x,y)$はROI$S$で一意に定まり、逆変換は安定である。

（条件1）$S=H\cup K$（$S$の内部のどの点においても、$f(x,y)$またはその点を通過する180度方向の$p(r,\phi)$が測定されている）

（条件2）$B\equiv H\cap K\neq\{\phi\}$（$S$の内部に$f(x,y)$とその領域を通過するすべての$p(r,\phi)$が（両方とも）測定されている領域$B$が存在する。ただし、$B$はいくら小さな領域であってもよい）

結果1と2の条件を満たす具体的なイメージングの設定を、**図2a～c**に示す。**図2b、c**の設定における解の一意性は結果1では証明することができず、結果2を使うと（$f(x,y)$が既知である領域$K$が大きい場合に）必要な投影データを結果1で示されるよりも大幅に削減することができる。

## インテリアCTの画像再構成

本章では、文献3～9において提案されたインテリアCTの画像再構成法について述べる。1番目の手法は、Interior問題の解の一意性を証明する数学的枠組みである微分逆投影（DBP：Differentiated Backprojection）の理論に基づくDBP-

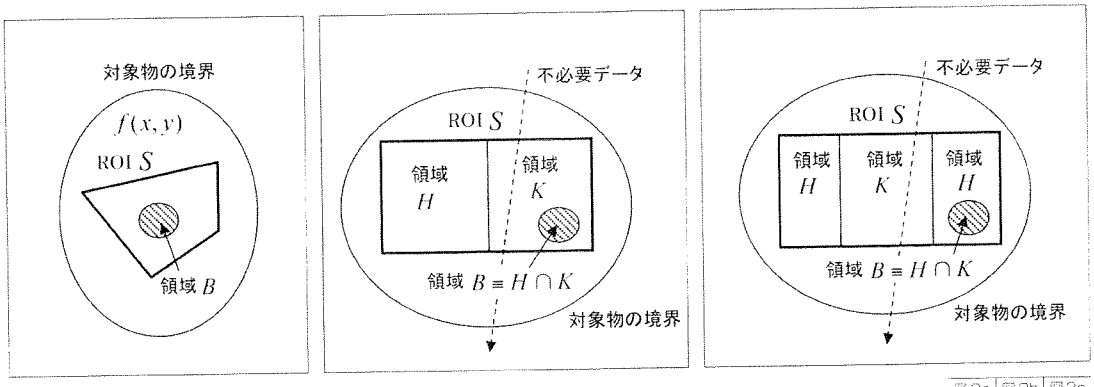


図2a | 図2b | 図2c

**図2 Interior問題の設定**
a：結果1で解の一意性が示されるinterior問題の設定
b、c：結果2で解の一意性が示されるinterior問題の設定

POCS（Projection Onto Convex Sets）法、2番目の手法はART法やMLEM法などの逐次近似法に、対象物$f(x,y)$がサポート（値が零でない領域）$O$の外側で零であることと、領域$B$、$K$で既知であることを拘束条件として組み込んだ拘束条件付き逐次近似法である。前章で述べたように、Interior問題において厳密な画像再構成を可能にするキーは$f(x,y)$がサポート$O$の外側で零であるサポート拘束と、$f(x,y)$が領域$B$、$K$で既知である先見的知識であり、これらの拘束条件を画像再構成の過程に組み込むことが重要である。

### 1) DBP-POCS法[3~7]

DBP-POCS法では、ROI$S$をHilbert Lineとよばれる直線の集合$L(u)$; $u \in U$（$u$は直線を表すパラメータ）に分解しておき、DBPを用いて画像再構成をHilbert Lineごとの Hilbert変換の逆問題に変換して再構成を行う。ただし、Hilbert Lineの集合$L(u)$; $u \in U$は、①ROI$S$の各点$(x,y)$が少なくとも1つのHilbert Line $L(u)$に属すること、②すべてのHilbert Lineは$f(x,y)$が既知である先見的知識を表す領域$B$と交わること、の2つの条件を満足するように選ぶ。具体的なROI$S$と先見的知識$B$の設定に対する典型的なHilbert Lineの取り方を**図3a**に示す。そして、各Hilbert Line $L(u)$ごとに以下の手順で画像再構成を行う。以降の説明では複雑さを避けるため、結果1に対応する**図2a**の設定を考えるが、結果2に対応する設定に拡張することは容易である。

(1) DBP：まず、Hilbert Line $L(u)$とROI$S$が交わるすべての点$(x,y)$について、次式のDBPを計算してHilbert画像$g_u(x,y)$を求める。

$$g_u(x,y)=\frac{-1}{2\pi}\int_0^{\pi} d\phi \frac{\partial}{\partial r} p(r,\phi)\Big|_{r=x\cos\phi+y\sin\phi} \mathrm{sgn}(\cos(\phi-\theta(u)))$$
$$(x,y)\in L(u)\cap S \quad \cdots\cdots\cdots\cdots\cdots\cdots (1)$$

ただし、$\theta(u)$は$L(u)$と$x$軸がなす角度を表す。なお、Interior問題ではROI$S$を通過する投影データ$p(r,\phi)$のみが利用できるため、$L(u)\cap S$の外側では投影データの角度欠損が生じてDBPを計算することができない。

(2) Hilbert逆変換：**図3b**に示すようにHilbert Line $L(u)$上に1次元座標$t$を定義して（原点は任意）、原画像$f(x,y)$を$f(t)$により表しHilbert画像$g_u(x,y)$を$g(t)$により表す。すると、$f(t)$と$g(t)$の関係は次式の1次元Hilbert変換で表されることがDBPの理論により知られている[3~7]。

$$g(t)=\frac{1}{\pi}\,\mathrm{p.v.}\int_a^b ds \frac{1}{t-s} f(s) \qquad t\in(b,e) \cdots\cdots\cdots (2)$$

ただし、p.v.は積分のCauchyの主値を表し、点$a$、

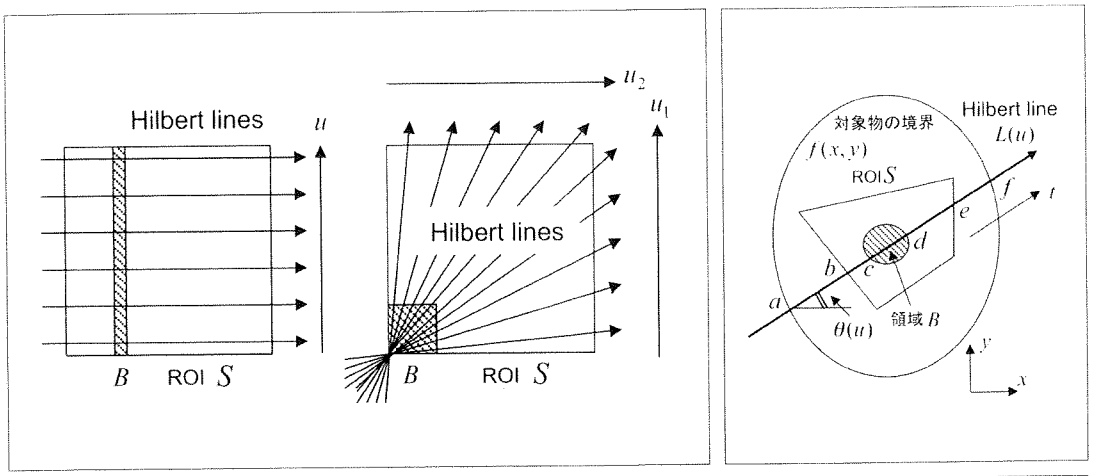


図3a | 図3b

**図3　Hilbert Line $L(u)$**
a：Hilbert Line $L(u)$の取り方の具体例
b：Hilbert Line $L(u)$上の座標系の定義

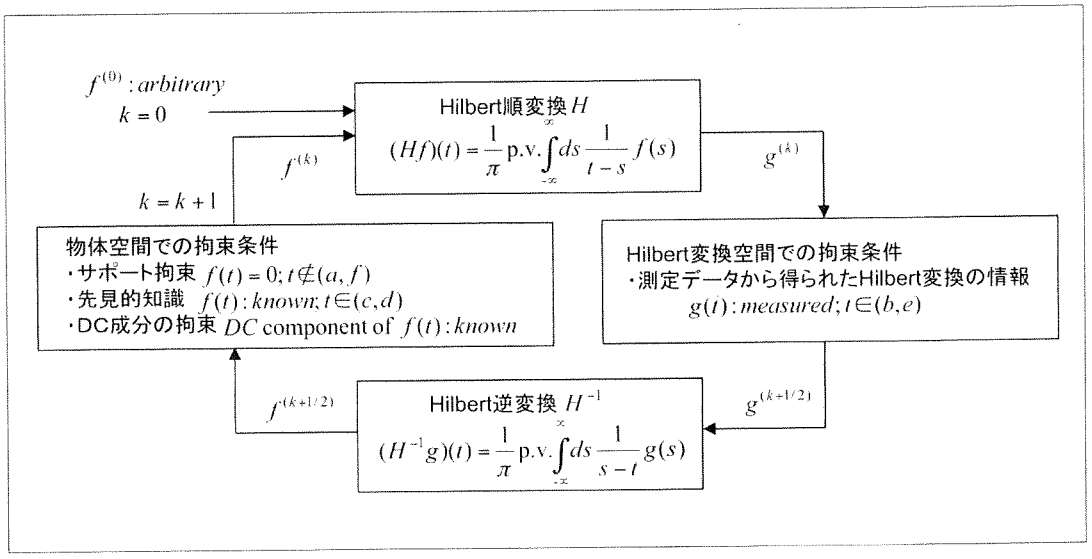


**図4　POCS法によるトランケーションHilbert逆変換のアルゴリズム**

$b$、$c$、$d$、$e$、$f$は**図3b**のように定義する。式（2）の積分変換の特徴は$f(t)$のサポートが$(a,f)$であるのに対し、$g(t)$はトランケーションされ一部区間$(b,e)$でしか観測されない点にあり、トランケーションHilbert変換とよばれている[3]。Hilbert Line $L(u)$上の画像再構成は式（2）の逆問題に帰着し、式（2）を$f(t)$について解くことで、再構成を行うことができる。

式（2）のHilbert変換の逆変換にはPOCS法とよばれる反復法を用いる。POCS法の処理の流れを**図4**に示すが、Hilbert変換の順変換$H$と逆変換$H^{-1}$をくり返し、画像$f(t)$の空間では①区間$(a,f)$の外側で$f(t)=0$となること、②領域$B$に対応する区間$(c,d)$で$f(t)$は先見的知識で与えられたも

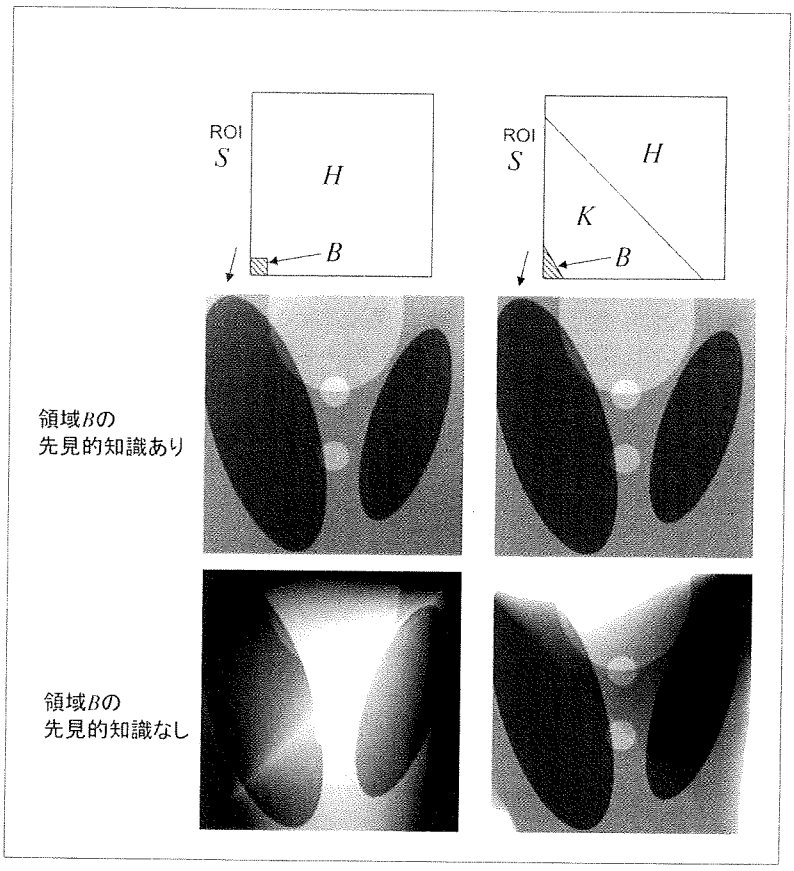


図5 DBP-POCS法によるShepp-Loganファントムの再構成画像
左：結果1で解の一意性が成り立つ設定
右：結果2で解の一意性が成り立つ設定

のと一致すること、③$f(t)$のDC成分はHilbert Line上の投影データであるから既知であること、の拘束条件を課し、Hilbert変換$g(t)$の空間では区間$(b,e)$で$g(t)$は投影データからDBPで求めたものと一致すること、の拘束条件を課す。POCS法の反復をくり返すと、$f(t)$はすべての拘束条件を同時に満足する解に収束し、このような$f(t)$は前章の解の一意性からROI$S$で一意に定まるため、正しく再構成できる。

DBP-POCS法で頭部CT実データを再構成した結果は文献2に示されており、ここでは図5にShepp-Loganファントムを用いて行った数値実験の結果を示す。Shepp-Loganファントム内部に正方形のROI$S$が存在する状況を想定した。右側は結果1で解の一意性が示される設定、左側は結果2で解の一意性が示される設定に対する再構成画像である。いずれも、上段が解の一意性を保証するのに必要な領域$B$の先見的知識を用いた場合、下段は用いない場合を表している。領域$B$の先見的知識がない場合には解が一意に定まらず、再構成画像にDCシフトや低周波アーチファクトが生じ、定量性が失われる。これに対して、領域$B$の非常に小さな先見的知識があれば、再構成画像の画質は劇的に改善される。

### 2) 拘束条件付き逐次近似法[3, 8, 9]

解の一意性と安定性が保証されれば、ART法やMLEM法などの逐次近似法を用いて画像再構成を行うことも可能である。文献3、8、9では逐次近似法によるトランケーションのある投影データからの画像再構成法が提案されたが、いくつか（必ずしも自明でない）注意すべき点があるので、以下に述べる。

(1) **再構成の手順**：まず、Interior問題に逐次近似法を適用した場合に、再構成の対象となり厳密な再構成が可能な領域はROI$S$のみであるが、逐次近似法を適用する際の画像マトリックスは、対象物$f(x,y)$を完全に含むように、大きく取る必要がある。すなわち、画像ベクトル$\vec{x}=(x_1,x_2,\cdots x_J)$は$f(x,y)$のサポート$O$を完全に含むように取り、投影データベクトル$\vec{y}=(y_1,y_2,\cdots y_I)$はROI$S$を通過する直線上の投影データのみを並べて作る。すると、式の数$I$が未知数の数$J$よりも少ない解が一意に定まらない連立一次方程式$\vec{y}=A\vec{x}$ができる。これを逐次近似法を用いて解き、最後に解$\vec{x}$のROI$S$の部分だけを取り出すと、正しい画像と一致する。これが正しい逐次近似法の適用手順である。ROI$S$のサイズによらず画像マトリクスを大きく取る必要があり、DBP-POCS法と比較して効率的な再構成法とはいえないが、この問題点を克服する手法は知られていない。

(2) **拘束条件**：Interior問題において厳密な画像再構成を可能にするキーは、$f(x,y)$がサポート$O$の外側で零であるサポート拘束と$f(x,y)$が領域$B$、$K$で既知である先見的知識であり、これらの拘束条件を反復計算の過程で使用しなければ正しい再構成を行うことはできない。拘束条件を組み込む手法としては、①各反復回数$k$における画像更新後に画像$\vec{x}^{(k)}$のサポート$O$外側の画素値を零に置き換え、領域$B$、$K$の画素値を先見的知識で与えられた値に置き換える、②連立一次方程式$\vec{y}=A\vec{x}$を作成する際に、サポート$O$外側の画素値は零で、領域$B$、$K$の画素値は先見的知識で与えられた値と仮定して未知数$\vec{x}$から除外する、の2つが考えられる。

**図6**に、上述の逐次近似法を適用して実際に画像再構成を行った結果を示す。文献3とほぼ同様な心臓イメージングの状況を想定し、図において点線の円がROI$S$を表し、実線の楕円がサポート拘束を課す領域$O$を表している。このように、ROI$S$が対象物の境界付近に位置する設定の場合、$O$の外部にあり$S$の内部にある（$(x,y)\notin O$かつ$(x,y)\in S$）領域$B$が存在すれば、その領域で$f(x,y)=0$となることが自動的に結果1における先見的知識$B$として使用されるため、『対象物$f(x,y)$の値が撮影前に既知である』という、いくぶん非現実的な仮定は不要となる。これは文献3で想定された問題設定で、Interior問題の特別な場合になっている。具体的な逐次近似法としては、OSEM法を上述のように修正した手法を用いた。再構成画像を見ると、領域$B$が存在し解の一意性が成り立つ設定（2、3列目）と、領域$B$が存在しない解の一意性が成り立たない設定（4列目）とでは、アーティファクトの量がかなり違うことがわかる。

さらに文献9では、上述の逐次近似法を発展させて、対象物のサポート$O$と先見的知識を表す領域$B$の位置が未知の場合に、これらを反復計算の過程で自動的に推定する機能をもつ逐次近似法が提案された。本手法によれば、『事前に対象物のサポート$O$と領域$B$の位置が既知である』といういくぶん非現実的な仮定も不要となる。

### 3) 雑音特性

インテリアCTと（トランケーションがない）完全な投影データを測定する通常のCTとで、再構成画像のSN比に違いがあるかを慎重に調べた。文献2の**図2**に例が示されているように、インテリアCTにおいて不必要な投影データを測定しないことに起因するSN比の低下は、無視できる程度で驚くほど小さい。

## おわりに

本論文では、インテリアCTを研究開発したい技術者や研究者向けに、筆者らの原著論文で提案されている画像再構成法について解説した。景気が悪いなどの理由から活力がなくなっている日本のメーカーに、ぜひ奮起して世界に先がけて『日本発のアイデアである』インテリアCTを実用化してもらいたい。

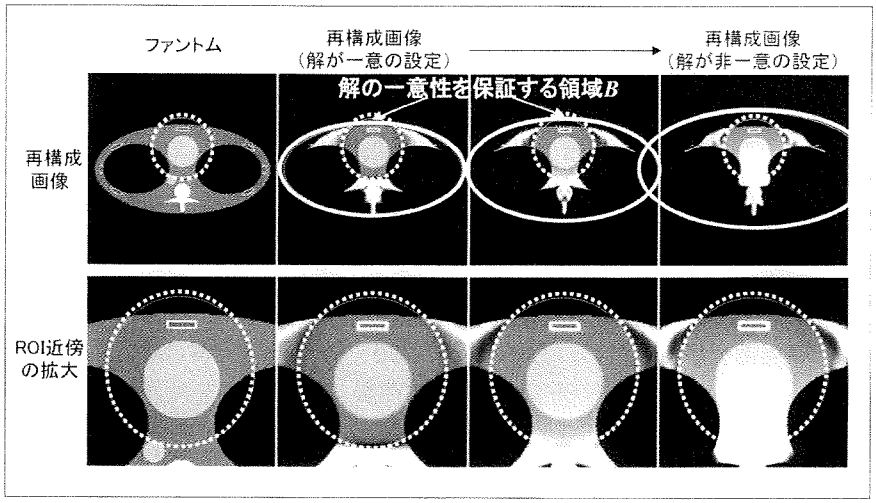


図6 拘束条件付き逐次近似法による再構成画像
(点線の円：ROI、実線の楕円：サポート拘束を課すのに用いた対象物の境界)

## 参考文献


1) 工藤博幸: 被曝量削減を目指した新しいCTの構成方式―関心領域X線照射方式の基礎―. 映像情報メディカル 37(13): 1408-1411, 2005
2) 工藤博幸: インテリアCTの提案. 映像情報メディカル 40(13): 1188-1193, 2008
3) Defrise M et al: Truncated Hilbert transform and image reconstruction from limited tomographic data. Inverse Problems 22: 1037-1053, 2006
4) Kudo H: Analytical image reconstruction methods for medical tomography－ Recent advances and a new uniqueness result－. Proceedings of Mathematical Aspects of Image Processing and Computer Vision 2006: Paper No. 00001652, 2006 (http://eprints.math.sci.hokudai.ac.jp/archive/00001652/2006)
5) Ye Y et al: A general local reconstruction approach based on a truncated Hilbert transform. Int J Biomed Imaging 2007: Article ID 63634, 2007
6) Kudo H et al: Tiny a priori knowledge solves the interior problem in computed tomography. Phys Med Biol 53(9): 2207-2231, 2008
7) Courdurier M et al: Solving the interior problem of computed tomography using a priori knowledge. Inverse Problems 24: Paper No. 065001, 2008
8) Zeniya T et al: 3D-OSEM reconstruction from truncated data in pinhole SPECT. Conference Record of 2007 IEEE Medical Imaging Conference: Paper No. M25-1, 2007
9) Rashed EA et al: Iterative region-of-interest reconstruction from truncated CT projection data under blind object support. 日本医用画像工学会誌 Medical Imaging Technology 27 (in printing)

特集／認知症診断の最前線

# MRI情報を用いた脳血流SPECT画像の解析と再構成
# Analysis and Reconstruction of Cerebral Blood-Flow SPECT Images Using MRI Information

工藤 博幸*
Hiroyuki KUDO

要 旨
筆者らは，同一患者のSPECT画像とMRI画像を融合して用い，脳の萎縮を伴わずに血流が低下している部位を検出する画像解析手法FUSEを開発した．FUSEは，現在実用化が進んでいる3D-SSPやSPMなどの統計学的画像解析法と比較して，1）正常人SPECT画像のデータベースを必要としないこと，2）脳形状個人差や脳萎縮の影響を受けにくいこと，の2つの利点がある．また，同一患者のMRI画像を事前情報として巧妙に利用して，SPECTの主要な画質劣化要因である部分容積効果や統計雑音の影響を軽減して病変を検出しやすい画像を生成する統計的画像再構成法を開発し，FUSEの性能を向上させることに成功した．本論文では，これらの研究について紹介する．
キーワード：認知症，脳血流，SPECT，MRI，画像解析，画像再構成

We developed an image analysis method called FUSE to detect blood-flow deteriorated regions from brain SPECT images by using MRI information. Compared to the conventional methods such as 3D-SSP and SPM, FUSE does not require a database consisting of SPECT images of normal volunteers, and its accuracy is hardly affected by the individual variation in brain morphology among a variety of patients and the existence of brain atrophy. We also developed a statistical image reconstruction method which is able to improve lesion detectability significantly by incorporating MRI information into the reconstruction process. This method combined with FUSE improved accuracy of the lesion detection. In this paper, we introduce these works.
**Key words:** Dementia, Cerebral blood-flow, SPECT, MRI, Image analysis, Image reconstruction
Med Imag Tech **28**(1): 19-25, 2010

## 1. はじめに

アルツハイマー病・脳血管障害・レビー小体型認知症（DLB）などの認知症の患者数は急速に増加してきており，大きな社会問題になっている．認知症の画像診断にSPECT／PETで撮影した脳血流画像を用いると，MRI画像上で脳の萎縮を伴わない初期段階で疾患を発見できる．しかし，初期段階での血流低下は微妙で医師が視覚的に判断しただけでは見落とす場合があり，定量的な画像解析に基づく計算機支援診断を導入することが望ましい．とくに，SPECT脳血流画像から血流低下部位を検出するソフトウェアとして，Minoshimaらが開発した3D-SSP（3-D Stereotactic Surface Projection）とFristonらが開発したSPM（Statistical Parameter Mapping）の実用化が進んでおり，臨床的有効性が確認されている〔1～3〕．しかし，3D-SSPやSPMに代表される統計学的画像解析法は患者と正常人のSPECT画像を比較する原理に基づいているため，(1) 性別・年齢・使用放射性薬剤・撮像装置・画像再構成法ごとに正常人SPECT画像のデータベースを構築しておく必要があること，(2) 脳形状個人差や脳萎縮の影響を受けやすいこと，などの問題点がある．

筆者らは，統計学的画像解析法に代わる新手法として，同一患者のSPECT画像とMRI画像を

* 筑波大学大学院システム情報工学研究科コンピュータサイエンス専攻〔〒305-8573 つくば市天王台 1-1-1〕：Graduate School of Systems and Information Engineering, University of Tsukuba.
e-mail: kudo@cs.tsukuba.ac.jp
論文受付：2009年11月4日
最終稿受付：2009年12月28日